CEA/SACLAY
DSM

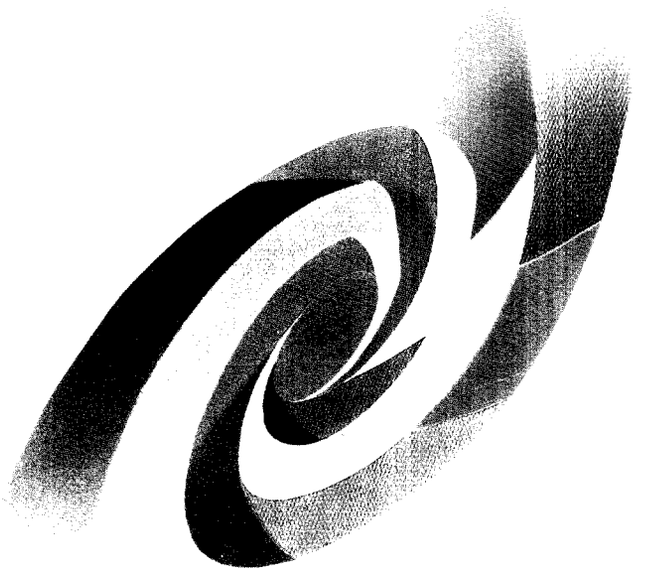

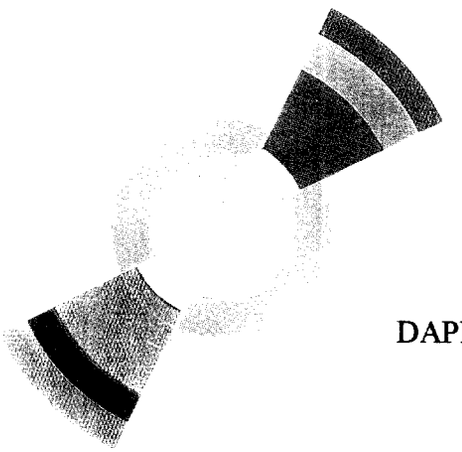

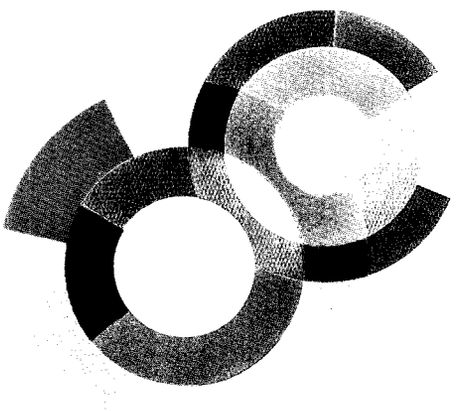

DAPNIA/SPhN-97-46 07/1997

Kaon Production in Nucleus-Nucleus Collisions at 92 MeV per Nucleon

DAPNIA

R. Legrain, J.F. Lecolley, F.R. Lecolley, N. Alamanos, L. Bianchi, Y. Cassagnou, H. Dabrowski, B. Erazmus, J. Julien, D. Lebrun, Ch. Le Brun, A. Mougeot, P. Hameau, G. Perrin, P. de Saintignon, J.L. Sida and J.P. Wieleczko

Département d'**A**strophysique, de Physique des **P**articules, de Physique **N**ucléaire et de l'**I**nstrumentation **A**ssociée
CEA/Saclay F-91191 Gif-sur-Yvette Cédex

Couverture Sylvie Cabrit et Marc Sauvage

Submitted to the Physical Review C

KAON PRODUCTION IN NUCLEUS-NUCLEUS COLLISIONS AT 92 MeV PER NUCLEON *

R. Legrain[a)], J.F. Lecolley[b)], F.R. Lecolley[b)], N. Alamanos[a)], L. Bianchi[c)], Y. Cassagnou[a)], H. Dabrowski[d)], B. Erazmus[d)], J. Julien[a,d)], D. Lebrun[e)], Ch. Le Brun[b)], A. Mougeot[a)], P. Hameau[a)], G. Perrin[e)], P. de Saintignon[e)], J.L. Sida[a)] and J.P. Wieleczko[c)].

a) CEA DAPNIA/SPhN, CE Saclay, 91191 Gif-sur-Yvette CEDEX, FRANCE.

b) LPC, ISMRA et Université de Caen, CNRS / IN2P3,

6 bld du Maréchal Juin, 14050 Caen CEDEX, FRANCE.

c) GANIL. BP 5027, 14021 Caen CEDEX. FRANCE.

d) SUBATECH, Université de Nantes / Ecole des Mines de Nantes, CNRS / IN2P3

4 rue Alfred Kastler, La Chantrerie, 44072 Nantes CEDEX 03, FRANCE

e) ISN Grenoble, 53 Avenue des Martyrs, 38026 Grenoble CEDEX, FRANCE.

(July 30, 1997)

Abstract

K^+ production far below the free nucleon-nucleon threshold has been investigated in collisions of ^{36}Ar on ^{12}C, ^{nat}Ti and ^{181}Ta targets at an incident energy of 92 MeV per nucleon. The cross sections for K^+ production have been inferred from the observed muon decays of positive kaons. The target dependence of cross sections is discussed and the results are compared to proton induced K^+ production and to subthreshold pion production experiments.

PACS numbers: 25.75.Dw, 25.70.-z

*Experiment performed at GANIL, Caen

I. INTRODUCTION

The meson production in heavy ion collisions at subthreshold energies offers the possibility to study dense and hot nuclear systems and thus possibly the underlying nuclear equation of state [1]. At incident energy per nucleon well below the free nucleon-nucleon threshold, nucleons have to undergo several collisions in the hot and compressed zone to gain by chance enough energy to make possible the meson production, or in a cooperative model, several nucleons have to pool their energy to produce the particles. Both processes are density and temperature dependent, so meson production can be a good probe of the early stages of the collision if the particle can escape the interaction zone without substantial final state interaction. In that respect, kaons, especially for K^+, seem to be particularly suitable since they have extremely low absorption and small scattering cross section with nucleons. K^+ production, in the elementary process $N + N \rightarrow K^+ + \Lambda + N$ requires an available energy of $E_0 = 670$ MeV, that is to say 1.58 GeV for an incident nucleon on a fixed target or 335 MeV for each nucleon. This makes very unlikely the K^+ production by first chance nucleon-nucleon collision at incident energies around 100 MeV/nucleon for which it has been shown that the pion production was in agreement with the simple participant-spectator collision geometry [2,3].

Another interest in K^+ production comes from the intrinsic nature of the kaon, since its production requires the associate production of a pair of strange quarks. Therefore subthreshold experiment on strangeness production may be related to the low but significant strange quark component in nucleons [4–6]. It is thus interesting to compare pion and kaon production in the same energetic conditions.

The K^+ production was measured more than ten years ago in Ne + NaF collisions at 2.1 GeV per nucleon [7], and only few data exist at subthreshold energies. An enhanced K^+ production compared to microscopic transport calculations has been found in $^{197}Au + ^{197}Au$ collisions at 1 GeV / nucleon [8]. Our first measurement of K^+ production in $^{36}Ar + ^{nat}Ti$ at 92 MeV / nucleon [9] is up to now the only result at an energy far below the free

nucleon-nucleon threshold. The order of magnitude of the cross section is in reasonable agreement with the systematics of meson production probabilities per participant nucleon as a function of the Coulomb corrected bombarding energy normalized to the production threshold in free nucleon-nucleon collisions [10]. It it has also been reproduced by two quite different theoretical calculations. One of these calculations is performed in the framework of a cooperative model which has already been applied to subthreshold pion production [11], while the other assumes an incoherent production mechanism and introduces fluctuations using the Boltzmann-Langevin approach with a soft equation of state [12].

In this paper, we report on new measurements of K^+ production using a beam of 92 MeV/nucleon ^{36}Ar. The experiment is described in section II. The data analysis methods are presented in section III and the results are discussed in section IV.

II. EXPERIMENTAL DETAILS

A. Kaon detection

In K^+ production measurements in heavy ions collisions around 100 MeV per nucleon, the K^+ energy is low and it is not possible to use magnetic detection and range telescope techniques as it is done at higher incident energies. However, it is still possible to detect kaon decays with no kaon energy threshold. But in this case, a total production cross section can only be inferred while the angular distribution and the kaon energy can not be measured.

The mean lifetime of the K^+ is 12.4 ns and the main decay channels are:

- $K^+ \rightarrow \mu^+\nu$ with a branching ratio of 64% and a muon kinetic energy $T_{\mu^+} = 153$ MeV for a decay at rest.

- $K^+ \rightarrow \pi^+\pi^0$ with a branching ratio of 21% and a pion kinetic energy $T_{\pi^+} = 110$ MeV for a decay at rest.

with mean life time of 12.4 ns.

The delayed particle (μ^+ or π^+) is detected in a range telescope designed to accommodate a high counting rate. But the branching ratio is higher for the muon decay channel and the range of a 153 MeV muon is larger than the range of a 110 MeV pion, allowing a better rejection of wrong events. The detection of kaons can be signed by the range and energy measurement of the delayed 153 MeV muons. The mean life time measurement provides an additional check. This method takes advantage of two interesting characteristics of the GANIL beams: the very high intensity available on a small beam spot (a few mm^2) and a well defined time structure (1 ns every 70 ns) which allows the measurement out of the beam burst with a reasonable number of triggers. The same detection method was used in the first K^+ production experiment performed at GANIL [9] while the same kaon decay method was used in proton induced K^+ production measurements [13].

B. Experimental setup

The experimental setup is sketched in Figure 1. A copper plate stopping kaons up to 40 MeV energy for normal trajectories was located close to the target, covering polar angles from 45 ° to 135 °. Muons from the kaon decays are detected in a range telescope located at 90° with respect to the beam direction.

The telescope is made of passive and active absorbers and consists of four parts:

1. passive absorbers of different nature are placed in front of the telescope in order to reduce the background counting rate in the first active planes of the telescope.

2. The trigger (T1-4) where a coincidence of the detection planes is required, and the trajectories may be checked in two hodoscopes (H1-2, H3-4). Plates of copper are inserted between trigger detectors in order to enlarge the matter thickness. The four active trigger planes are segmented in forward and backward parts.

3. Just behind, the muons of interest are stopped in the eight absorbers (A1 to A8, 2 and 4 cm thick), allowing the measurement of the range, the specific energy loss and

the residual energy of stopping particles. The absorber planes are segmented in four parts.

4. The last detection plane is used as a veto to reject energetic cosmic muons crossing the whole telescope.

All detectors have been tuned and energy calibrated using cosmic ray muons.

C. Simulation

The whole detector geometry has been entered in a simulation using the GEANT package from CERN library [14]. The emission of the kaons is assumed to be isotropic from the center of the target. Muons from the decay of kaons are then selected and tracked trough the detector. The energy loss spectra of all scintillators are constructed. The resulting range and energy distributions are shown on Figure 2 for the expected experimental statistics. The total energy detected in the active parts of the telescope ($\simeq$ 55 MeV) is a significant part of the muon energy (152.9 MeV). The total efficiency of the detection system has been extracted from this simulation for different velocities and energy distributions of the primary kaon source. The simulation yields a total efficiency around 0.7 %. More details on the results of these calculations will be given in section IV.

D. Experiment

The experiment has been performed at the GANIL National Laboratory using a $\simeq$ 200 nAe ^{36}Ar beam and ^{12}C, ^{nat}Ti and ^{181}Ta targets 102 mg/cm^2, 92 mg/cm^2 and 79 mg/cm^2 thick respectively. The range telescope was centered at 90 ° with respect to the beam direction. The beam pipe and some mechanical parts close to the target were made of low Z material in order to limit the background counting rate. A parasitic beam has been used to determine the nature, thickness, and position of the absorbers in front of the telescope and in between the trigger planes. Several configurations have been tested. The

final configuration was chosen in order to accommodate the highest beam current with the lowest counting rate. The on-line trigger condition requires the coincidence of H3-4, T1 T2, T3, T4 and A1 planes. A time measurement of the trigger plane T3 with respect to the beam time structure (accelerator R.F.) was performed. The timing of the Cyclotron RF was checked continuously with an independent scintillator. For each target, data were accumulated with a gate rejecting prompt events, but runs including prompt events have been periodically performed.

III. DATA ANALYSIS

A. Events selection

The muonic kaon decay events are identified by using the energy loss informations from the telescope. At each step of the analysis, the time distribution of the selected events is compared to the kaon decay. The off line data reduction has been performed in two steps. Most of the background events are rejected in the first stage by the following selections :

1. Only delayed particles, with time arrival into the T3 counters larger than at least 3 ns with respect to the beam spill, are considered to reject prompt events.

2. A narrow time coincidence is applied to all planes to reject random events.

3. The measured energy losses in each counter of the trigger part are inside an energy window defined on the lower part by the cosmic muon at the minimum of ionization and on the higher part, by the values calculated for protons.

4. The triggering conditions are still satisfied when requiring only one hit per detection plane.

This first selection yields about 700 events for the three targets. The time distribution of these events is shown on Figure 3 as the remnant population of events after a delayed time

T_0. The solid line represents the expected slope for kaon decay. It is clear that the selection of kaon decay events has to be more efficient.

In a second stage, the muons from kaon decays are identified taking into account the energy losses in the absorber part of the telescope. Only events with a total energy deposited in the active part of the telescope larger than 30 MeV are selected. A two dimensional cut, corresponding to the energy losses of the muons deduced from the simulation, is then applied to the two last counting scintillators.

The range and deposited energy distributions resulting from such a procedure are presented in Figure 4. These spectra represents the summ of the data obtained for the three targets studied in this experiment. Comparing these results to the simulation of Figure 2, it is clear that kaon decays have been observed.

The time distribution of the remaining events after the second step of the analysis for the three targets is shown in Figure 5. The solid line represents the expected slope for kaon decay. The measured time distribution is in agreement only with kaon decay after 18 ns. For $T_0 \leq$ 5ns prompt events are still present and a dead time effect due to the high counting rate for prompt events extends up to 18 ns. This dead time effect is reproduced by a simulation shown also in Figure 5 with a dead time equal to 80 % for $T_0 \leq$ 18ns. In Figure 6 are shown the time decay spectra observed with the ^{12}C, ^{nat}Ti and ^{181}Ta targets for $T_0 >$ 15 ns. These spectra seem compatible with kaon time decay spectra represented by solid lines in Figure 6. This is confirmed by the fits to the decay curve $N_0 exp(-t/\tau)$ performed for the three spectra for $T_0 >$ 18 ns which yield $\tau = 18.\ ns \pm 12.\ ns, 11.5\ ns \pm 4.3\ ns, 10.6\ ns \pm 2.6\ ns$ for the ^{12}C, ^{nat}Ti and ^{181}Ta spectra respectively. Subsequently the mean life of the kaon (τ = 12.4 ns) has been used to derive the number of produced kaon N_0 from the number of counts observed in the interval 18 - 50 ns. This gives N_0 = 23, 51, and 60 for ^{12}C, ^{nat}Ti and ^{181}Ta respectively. The statistical uncertainty on these numbers has been estimated using a simulation. For each target, 10 000 time decay spectra have been generated with an initial number of counts equal to N_0 and a mean lifetime 12.4 ns. Then a distribution of the estimated initial number of counts N_0^{est} has been obtained from the number of counts in the

interval 18 - 50 ns. To get an approximation of a standard deviation of these discrete N_0^{est} distributions, the next N_0^{est} value corresponding to a value lower than 60% of the maximum of the distribution has been used. The results are reported on table I.

B. Decorrelated analysis

An analysis based on the data reduction of the total energy spectrum has been performed in order to check the values extracted from the event by event analysis. The energy spectrum is composed of good events superimposed on a contamination background which can be estimated using decorrelation techniques. The first selection leads to a first sample of about 700 events. Starting from this first sample, we construct eight classes of events associated with each stopping absorber number (A_1 to A_8). For an event of a given class with a decay time $T > T_0$, we construct a decorrelated event by a random sampling (excluding the parameters of the physical event) of the energy loss in the detection planes. All the events are treated in the same way, so we obtain a decorrelated energy distribution associated with a decay time $T > T_0$. This distribution is normalized to the lower part of the initial energy distribution ($\approx 25MeV$) where the muons of interest are not expected. The two energy spectra are subtracted allowing to evaluate a number of counts with a decay time $T > T_0$. The time spectrum deduced from this method is presented in Figure 7. The global features of the time spectrum are similar for both analysis (event-by-event: figure 5 and decorrelated: figure 7). Let us now parametrize the time spectra by $N_0 exp(-t/\tau)$.Then $N_0 = 143. \pm 53.$ and $\tau = 14.6 \pm 3.0$. The full line in Figure 7 is the result of this exponential fit. The event number N_0 is compatible with the number of good events (134) deduced from the previous analysis. From this result one can conclude that there is no loss of events and no background contamination in our data selection. The fitted slope parameter τ is also compatible with the expected slope for K^- decay: $\sim 12.4ns$. The convergent results of both methods give some confidence about the extracted number of events.

IV. RESULTS AND DISCUSSION

A. Derivation of cross sections

In order to extract production cross sections, the K^+ detection efficiencies have been calculated from GEANT simulations including a geometrical description of the experimental set-up and assuming three different production modes:

1. Isotropic emission in the lab frame with a kinetic energy T_K =35 MeV.

2. Isotropic emission in the lab frame with a kinetic energy spectrum reported elsewhere [11].

3. Isotropic emission in the fireball frame with a kinetic energy T_K=35 MeV.

In the above dtection efficiencies, corrections for the particle decay are also included. The obtained total cross sections are presented in Table II and labeled 1, 2, 3 according to the three different production modes described previously. The values in brackets are the upper and lower limits of the total cross sections which take into account the statistical errors. The total cross sections are very little influenced by the assumed emission patterns and remain inside the limits of experimental errors independantly of the kaon energetic distribution and the Jacobian effects. Figure 8 shows the target mass dependence of the total cross section. It can be seen that the data are well described by a $A_T^{3/2}$ dependence and differ from the normal scaling $A_T^{2/3}$ observed in π production in the same energy range. In meson production analysis, it is usual to present experimental cross section in terms of probability per participant nucleon. This probability is given by:

$$P_i = \frac{\sigma_{\mathrm{exp}}}{\sigma_g < A_p >}$$

with σ_{exp} being the experimental cross section, σ_g the geometrical cross section and $< A_p >_b$ the mean number of participant nucleons. The geometrical cross section is expressed as:

$$\sigma_g = \pi r_0^2 (A_P^{1/3} + A_T^{1/3})^2$$

with A_P and A_T the mass numbers of the projectile and target nuclei, (r_0 = 1.2 fm) and

$$< A_p >= \frac{A_P A_T^{2/3} + A_T A_P^{2/3}}{(A_P^{1/3} + A_T^{1/3})^2}$$

The probabilities for kaon production are shown in Figure 9 as a function of the total available energy in the center of mass. The solid line shows the variation of the 2-body phase space volume. Starting from the absolute threshold (671 MeV) where full collectivity is needed, the kaon production follows the variation of the 2-body phase space and this trend seems to extend to more than 1 GeV above the threshold. The kaon production near the threshold seems to be governed by this phase-space behavior.

B. Comparison with existing data

Similarities in the subthreshold production of strange and non strange mesons can be seen with the universal dependence of the meson production probability per participant nucleon, if this probability is plotted as a function of the Coulomb corrected bombarding energy per nucleon normalized to the energy threshold in free N-N collisions [10].

The excitation function for π and K^+ production in A + A collisions is presented on figure 10. Our data (full stars) follow the trend given by previously measured data (π and K^+) [7,15–27]. The probability per participant nucleon to produce either a pion or a kaon is very similar at equivalent relative energy $[(E - V_C)/A]/E_{Th}^{NN}$ whatever the strangeness of the meson.

An analysis of π and K^+ production in p-nucleus reactions near the absolute threshold (140 MeV for π and 671 MeV for K) leads to a rather different conclusion. Using the same representation, we observe (Figure 11) a large gap between the two excitation functions. The ratio of the production probabilities in p+ Pb $\rightarrow \pi^0$ and p + Pb $\rightarrow K^+$ is about 10^3 and is comparable to the cross section ratio of the elementary processes N + N $\rightarrow$ N + N + π and N + N $\rightarrow$ N + Λ + K. Thus, the π and K production for p-nucleus collisions near the absolute threshold can be explained as a convolution of the elementary cross section

of the p-nucleon system using high momentum components of the nuclear wave function [1,28–30].The K^+ production results from a dominant two-step mechanism [28,30] in the collision of secondary pions (p+N $\rightarrow \pi$ + ..) with the nucleons inside the nucleus (π + N $\rightarrow \Lambda + K^+$). From these results, we would like to conclude that π and K productions in p-nucleus reactions are dominated by the N-N elementary process.

In the heavy-ion case, the similarities in the excitation functions (figure 10) of sub-threshold production of strange and non strange mesons allow to rule out a common N-N production mechanism. In that case, K^+ and π production at bombarding energies of 92 MeV/nucleon and 20 MeV/nucleon respectively would be comparable, considering the ratios between the incident energy per nucleon and the N-N production energy threshold. But in a 20 MeV/nucleon collision, the available energy in the N-N system is about 140 MeV when taking into account an internal momentum of 350 MeV/c (Figure 12). Then the sub-threshold pion production is energetically possible. However in a 92 MeV/nucleon collision, with the same internal momenta, the available energy is about 210 MeV, far from the kaon center-of-mass threshold energy ($\cong$ 671 MeV). This value is reached only by taking into account an internal momentum of 800 MeV/c in both partner nuclei (Figure 12). These estimations have been made in the most favorable kinematical configuration: a collision between a projectile nucleon with an internal velocity vector (beam + Fermi) aligned with the relative velocity and a target nucleon with a Fermi velocity in the opposite direction. The distribution of the internal momentum of nucleons in a nucleus deduced from experimental distributions [31] fall down about 3 orders of magnitude from P_f=350 MeV/c to P_f=800 MeV/c. In the case under consideration the probabilities to produce K^+ and π cannot be of the same order of magnitude. Additionally, large fluctuations of the one-body momentum distribution [12] cannot explain the scaling behavior of the K^+ and π excitation functions in A + A collisions. At energy as low as 25 MeV/nucleon, the simple Fermi motion cannot explain the measured cross section [32]. There is a need to call for cooperative modes of several participant nucleons to satisfy energy conservation [33,34]. Although, it is difficult to estimate the relative part of incoherent and coherent pion production processes, experi-

mental data [2,3,35,36] suggest that pions are emitted from a composite system formed by the overlap between the projectile and the target nuclei using the geometrical concepts of the fireball participant-spectator model [37]. Then, the size of the composite system is a function of the impact parameter. The pion production is possible only if the CM energy of the composite system(excitation energy) is such that $E^* \geq m_\pi$. This involves an upper limit for the impact parameter (b_{eff}) which is determined by energetic considerations.

The mean number of participant nucleons averaged over the impact parameters is respectively 10., 20., 39. for ^{12}C, ^{48}Ti, ^{181}Ta targets and ^{36}Ar projectile. The mean value of the CM energy is respectively 215., 435. and 715. MeV. The mean CM energy of the participants is given by:

$$< E_{cm} >= (m^2 < N_{pt} >^2 + 2mE_{lab} < N_p >< N_t >)^{1/2} - m < N_{pt} >$$

with $< N_p >$,$< N_t >$ respectively the mean number of participant projectile and target nucleons (m=931.5 MeV, $< N_{pt} >=< N_p > + < N_t >$ and $E_{lab} = 92MeV/nucleon$). The mean CM energy of the participants is lower than the kaon production absolute energy threshold ($671MeV$), except for the heaviest system. But the CM energy of the participants depends on the impact parameter:

$$E_{cm}(b) = (m^2 N_{pt}(b) + 2mE_{lab} N_p(b) N_t(b))^{1/2} - mN_{pt}(b)$$

$N_p(b)$ and $N_t(b)$ are calculated using the geometrical concepts of the fireball participant-spectator model [37]. This dependence is shown in Figure 13. By requiring that the CM energy is such that $E_{cm}(b) \geq 671$ MeV, we obtain upper limits for the impact parameter b of $b_{eff}/(R_p + R_t)$ =0.22, 0.54, 0.70 for ^{12}C, ^{48}Ti, ^{181}Ta targets respectively. Weighting with $b(b = 0 \rightarrow b_{eff})$, it is possible to evaluate the mean number of participating projectile and target nucleons in the range $0 \rightarrow b_{eff}$ which is determined by energetic considerations. In Table III, the calculated results for $< E_{cm} >$,$< N_{pt} > and < \varepsilon^* >=< E_{cm}/nucleon_{pt} >$ are shown for our three systems. In the last column of table III, the kaon production probabilities defined as $P_{eff} = \sigma_{exp}/(\sigma_{eff} < N_{pt} >_{eff})$ are reported ($\sigma_{eff} = \pi b_{eff}^2$).

For the three systems, the mean excitation energies of the composite system are similar. The cross section increases with the size of the intermediate zone, but the probability remains constant in the limit of experimental errors. In view of the uncertainties of fixing b_{eff}, the correlation between excitation energy and production probability gives support to the validity of the geometrical concepts used to define the assumed kaon sources. In spite of the uncertainties in the evaluation of $< \varepsilon^* >$, and in the estimation of the relative part of incoherent and coherent pion processes, an energy scaling is also observed in the pion production probability (Figure 14). This representation leads to a ratio $K/\pi \simeq 10^{-6}$ at $< \varepsilon^* > \simeq 20$MeV which is consistent with a model [11], where production cross sections are calculated in the framework of a cooperative mechanism. In this representation lower probabilities are associated to strange mesons (K^+) production in nucleus-nucleus collisions compared to non strange mesons (π) production, as it is observed in N-N and in p-A collisions.

Let us come back to Figure 10. The universal dependence of the meson production probability is disquieting in so far as the normalization to the energy threshold in free N-N collisions suggests that the N-N process is dominant. It is worthwhile to note that the universality is not strongly dependent on the definition of the probability. This is illustrated in Figure 15 where t calculated probabilities in several ways are presented. The general trends are similar whatever the used prescription. It is not surprising for the first two (Figs 15a,15b), when the bombarding energy increases: $b_{eff} \rightarrow b_{max} = (R_p + R_t)$. The probability defined as $\sigma_{exp}/\sigma_{eff}$ (Fig. 15c) and the scaled cross section (Fig. 15d) present also an universal behavior. When discussing subthreshold meson production in heavy ion rections, we bear in mind that the definite threshold in a fully coherent production is given by:

$$E_{th}^{def} = \frac{E_{th}^2 + 2(A_p + A_t)mE_{th}}{2mA_pA_t}$$

where $E_{th} = 140$ and 671 MeV respectively for pion and kaon productions. Then we observe that:

$$\frac{(E_{th}^{def})^\pi}{(E_{th}^{def})^K} \sim \frac{(E_{th})^\pi}{(E_{th})^K} \sim \frac{(E_{th}^{NN})^\pi}{(E_{th}^{NN})^K}$$

The observed universality is mainly due to the weak variation of the π and K threshold ratio with respect to the production energetic conditions. Thus the agreement of our data with the universal dependence of meson production [10] does not allow to conclude about the involved processes leading to meson production but is very useful to predict experimental cross sections.

V. CONCLUSIONS

Kaon decays have been observed in the collisions of 92 MeV/nucleon ^{36}Ar with ^{12}C, ^{nat}Ti and ^{181}Ta, and values of the total kaon production cross section have been derived using an event by event analysis and assuming isotropic emission. A statistical analysis applying correlation techniques to the various energy loss measurements shows that significant loss of events or background contamination can be excluded. The variation of the K^+ production cross section with target mass number follows a $A_T^{3/2}$ scaling law, much larger than the $A_T^{2/3}$ one observed for the pion production. This may indicate that the production does not deal with the volume and reflect the available excitation energy. As a function of the available energy, the K^+ production cross section roughly follows the two body phase space variation. The target dependence of two calculations [11,12] reproducing the order of magnitude of the cross section for the titanium target, remains to be investigated. Our results follow the general trend given by the universal dependence of meson production [10] for different definitions of the probability. But considering pion and kaon production in nucleon-nucleus collisions, a clear difference compatible with nucleon-nucleon production taking into account reasonable fermi momentum, is evident. This apparent discrepancy may be explained by assuming that in nucleus-nucleus collisions, the meson production occurs in the hot projectile and target overlapping zone. In that case, close to the absolute threshold, a cooperative mechanism is required and energetic conditions apply to the effective number of nucleons involved in the production. If the production probability is restricted to this effective number of nucleons involved in the process, the kaon production probability is

lower than the pion production probability as in nucleon-nucleus reactions. But the exact production process is still unknown. In this experiment, we have demonstrated that kaon production is measurable at incident energies below 100 MeV/nucleon. At such a low energy, geometrical and kinematical constraints play a major role in the kaon production.

REFERENCES

[1] W. Cassing, V. Metag, U. Mosel and K. Nita, Phys. Rep. **188**, 363 (1990).

[2] D. Lebrun et al., Phys. Lett. **B223**, 139 (1989).

[3] J.L. Laville et al., Nucl. Phys. A **564**. 564 (1993).

[4] J. Ellis and M. Karliner, Phys. Lett **B341**, 397 (1995).

[5] K. Abe et al, Phys. Rev. Lett. **74**, 346 (1995).

[6] D. Adams et al., Phys. Lett **B329**, 399 (1994).

[7] S. Schnetzer et al., Phys. Rev. Lett. **49**, 989 (1982).

[8] D. Miskoviec et al., Phys. Rev. Lett. **72**, 3650, (1994).

[9] J. Julien et al., Phys. Lett. **B264**, 269 (1991).

[10] V. Metag, Prog. Part. Nucl, Phys. **30**, 75 (1993).

[11] S. Gosh, Phys. Rev. C **45**, R518 (1992).

[12] M. Belkacem, E. Suraud and S. Ayik, Phys. Rev. C **47**, R16 (1993).

[13] V. P. Koptev et al. , Sov. Phys. JETP **67**, 2177 (1988).

[14] R. Brun et al., CERN Report No. DD/EE/84-1 (unpublished).

[15] E. Grosse, Prog. Part. Nucl. Phys. **30**, 89 (1993).

[16] M. Prakash, P. Braun-Munzinger and J. Stachel, Phys Rev C **33**, 937 (1986) and references therein.

[17] G. Sanouillet et al., Nuov. Cim. **99**, 875 1988).

[18] S. Y. Yung et al., Phys. Rev. Lett. **40**, 292 (1978).

[19] A.Sandoval et al., Phys. Rev. Lett. **45**, 874 (1980).

[20] K. A. Frankel et al., Phys. Rev C **32**, 975 (1985).

[21] E. Chiassa et al., Nucl. Phys. A **422**, 621 (1984).

[22] V. Bernard et al., Nucl. Phys. A **423**, 511 (1984).

[23] S. Nagamiya et al., Phys. Rev C **24**, 971 (1981).

[24] G. R. Young et al., Phys. Rev C **33**, 742 (1986).

[25] P. Braun-Munzinger et al., Phys. Rev. Lett **52**, 255 (1984).

[26] H. Heckwolf et al., Z.Phys. A **315**, 243 (1984).

[27] H. Noll et al., Phys. Rev. Lett. **52**, 1284 (1984).

[28] A.A. Sibitsev and M. Büsher, Z.Phys. A **347**, 191 (1994).

[29] W. Cassing et al., Proc. of the 7^{th} Int. Conf. on Nuclear Reaction Mechanisms, Varenna (1994) 544.

[30] M. Debowski et al., Z.Phys. A **356**, 313 (1996).

[31] J.V Geaga et al., Phys. Rev. Lett. **45**, 1993 (1980).

[32] J. Stachel et al., Phys. Rev C **33**, 1420 (1986).

[33] R Shyam and L. Knoll, Nucl. Phys. A **426**, 606 (1984).

[34] C. Guet and M. Prakash, Nucl. Phys. A **428**, 1196 (1984).

[35] B. Erazmus et al., Nucl. Phys. A **481**. 821 (1988).

[36] D. Lebrun et al., Z.Phys. A **335**. 73 (1990).

[37] J. Gosset et al., Phys. Rev C **16**. 629 (1977).

FIGURES

FIG. 1. Sketch of the experimental apparatus. Hodoscopes were labelled H, triggers T. Different materials are represented by different shading as indicated.

FIG. 2. simulation of the range and energy deposited in the absorbers for muons coming from the desintegration of K^+.

FIG. 3. time distribution obtained after the first selection (see text). the solid line corresponds to the time decay of K^+. This selection in insufficient to extract the muons correlated to this decay.

FIG. 4. Observed range and energy deposited in the absorbers for the complete selection. These spectra are a summation of the statistics for the three targets.

FIG. 5. Time distribution obtained for the complete selection (upper part) and for a simulation (lower part). the solid line corresponds to the time decay of K^+. Prompt events generate a dead time up to 18 ns that is introduced in the simulation.

FIG. 6. Time distribution obtained for the three targets for time larger than 15 ns. The solid line corresponds to the time decay of K^+.

FIG. 7. Time distribution obtained by a different analysis (see text) based on a global data reduction of the energy spectra.

FIG. 8. Cross section values extracted from our measurement as function of the target mass. The solid lines correspond to different evolutions with the target mass.

FIG. 9. Kaon production per participant nucleon as a function of the available energy. the solid line represents the evolution of the two body phase space volume.

FIG. 10. Meson production probability per participant nucleon as a function of square root of the Coulomb corrected bombarding energy per nucleon normalized to the energy threshold in nucleus-nucleus collisions.

FIG. 11. Pions and kaons production probability as a function of the square root of the Coulomb corrected bombarding energy per nucleon normalized to the energy threshold in the reaction $p + {}^{208}Pb$.

FIG. 12. Correlation of the incident beam energy and of the internal momentum of nucleus in both nuclei necessary to produce a pion or a kaon.

FIG. 13. Excitation energy of the fireball as a function of the impact parameter of the ${}^{36}Ar + {}^{181}Ta$ (a), ${}^{36}Ar + {}^{\mathrm{nat}}Ti$ (b) and ${}^{36}Ar + {}^{12}C$ (c) reactions at 92 MeV/nucleons. The absolute energy threshold to produce a kaon (671 MeV) is indicated by a solid line.

FIG. 14. Meson production probability per participant nucleon as a function of the effective excitation energy ϵ^* defined in the text.

FIG. 15. Different definitions of the probability to produce mesons as a function of the square root of the Coulomb corrected bombarding energy per nucleon normalized to the energy threshold.

TABLES

TABLE I. Number of kaon production events derived for the three measurements on ^{12}C, ^{nat}Ti and ^{181}Ta targets

target	^{12}C	^{48}Ti	^{181}Ta
N_0	23	51	60
	$(14 \rightarrow 37)$	$(37 \rightarrow 69)$	$(42 \rightarrow 79)$

TABLE II. Cross sections for K^+ production for the ^{12}C, ^{nat}Ti and ^{181}Ta targets for three asumptions. 1) Isotropic emission in the lab frame with a kinetic energy T_K =35 MeV, 2) Isotropic emission in the lab frame with a kinetic energy spectrum given by the reference 11, 3) Isotropic emission in the fireball frame with a kinetic energy T_K=35 MeV.

target	Ecm (MeV)	$\sigma_{tot}^{(1)}$ (pb)	$\sigma_{tot}^{(2)}$ (pb)	$\sigma_{tot}^{(3)}$ (pb)
^{12}C	820.	82.	96.	107.
		(50. $\rightarrow$ 131.)	(58. $\rightarrow$ 154.)	(65. $\rightarrow$ 172.)
^{48}Ti	1870.	511.	598.	571.
		(371. $\rightarrow$ 691.)	(434. $\rightarrow$ 808.)	(414. $\rightarrow$ 722.)
^{181}Ta	2744.	3093.	3616.	3358.
		(2165. $\rightarrow$ 4072.)	(2531. $\rightarrow$ 4761.)	(2351. $\rightarrow$ 4421.)

TABLE III. Characteristics of the the reactions of ^{36}Ar on ^{12}C, ^{nat}Ti and ^{181}Ta at 92 MeV/nucleon.

target	$< N_{pt} >$	$< E_{cm} >$	$< \varepsilon^* >$	P_{eff}
		MeV	MeV/nucleon	
^{12}C	33.7	696.	20.7	$(3.9 \pm 1.8)10^{-11}$
^{48}Ti	49.3	1090.	22.6	$(1.6 \pm 1.1)10^{-11}$
^{181}Ta	73.8	1439.	19.5	$(2.4 \pm 0.6)10^{-11}$

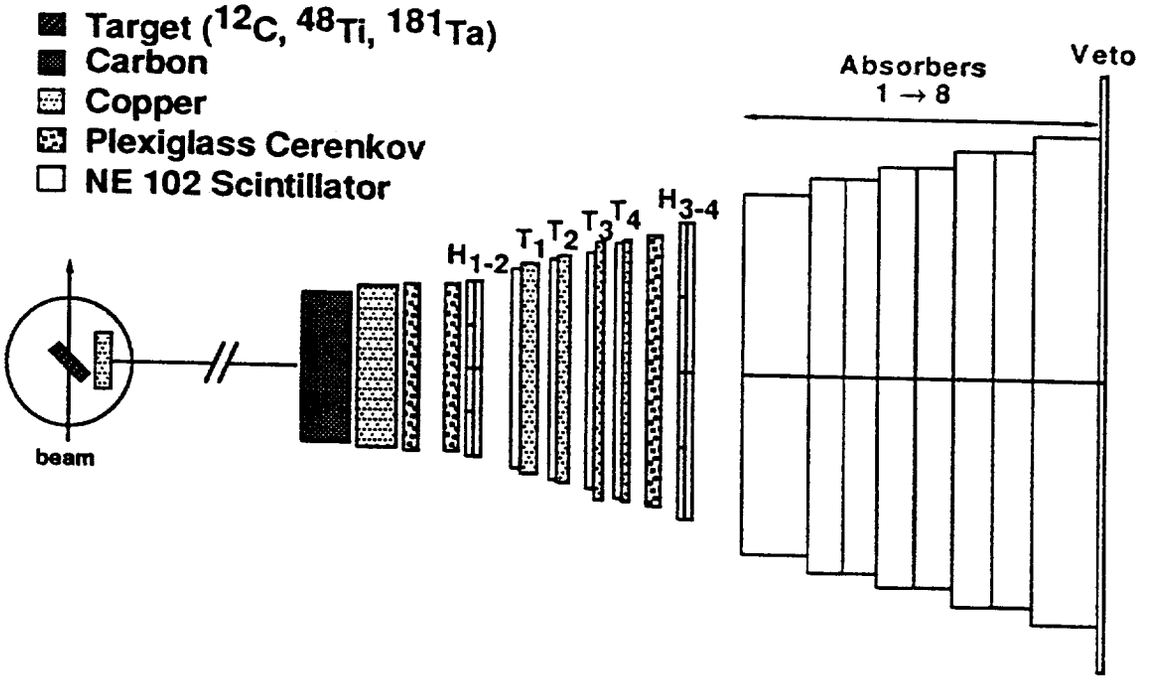
Target (^{12}C, ^{48}Ti, ^{181}Ta)
Carbon
Copper
Plexiglass Cerenkov
NE 102 Scintillator
Absorbers
1 → 8
Veto
H_{1-2}
T_1
T_2
T_3
T_4
H_{3-4}
beam

Fig. 1

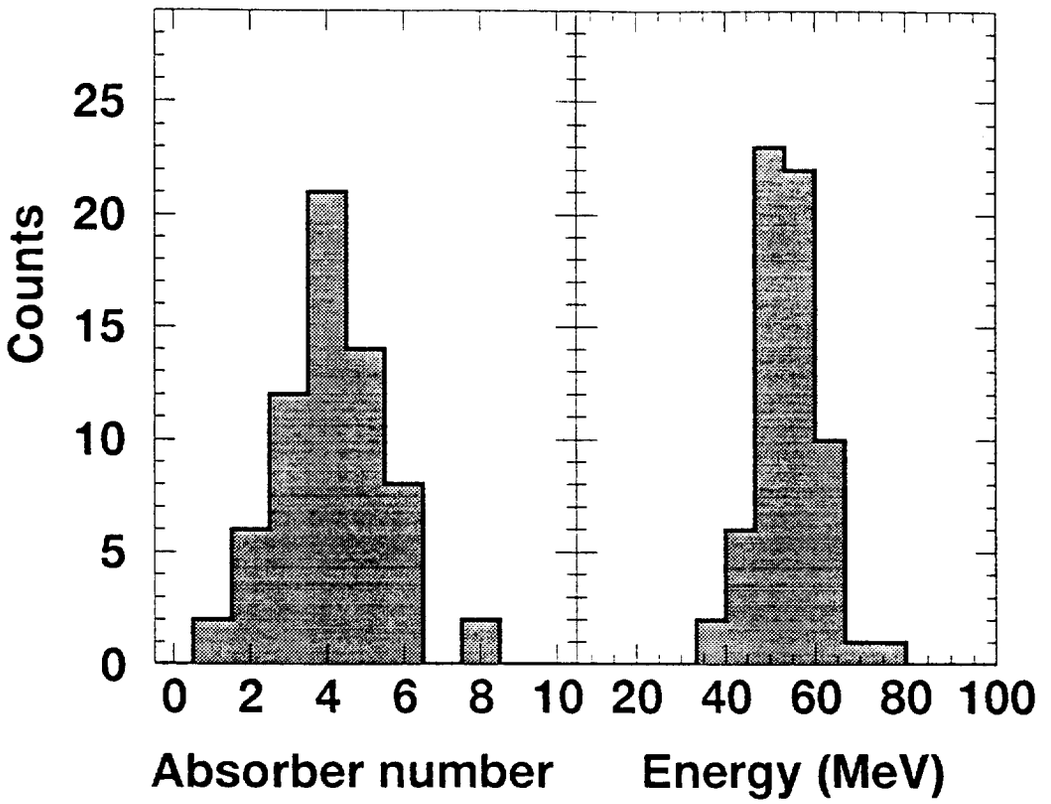
Counts
25
20
15
10
5
0
0 2 4 6 8 10 20 40 60 80 100
Absorber number
Energy (MeV)

Fig. 2

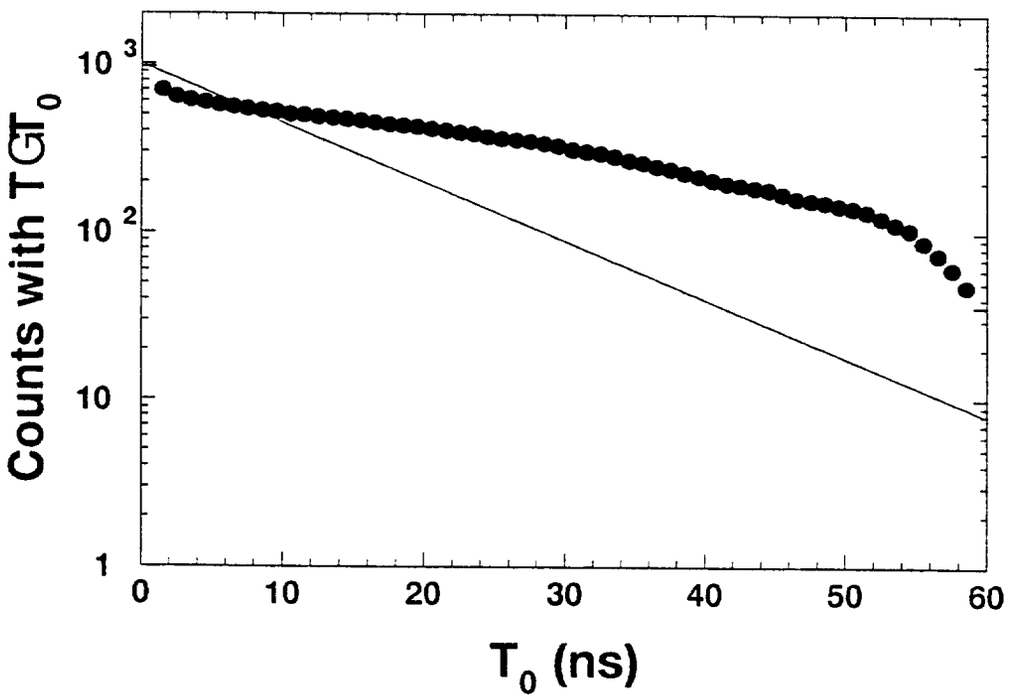

Fig. 3

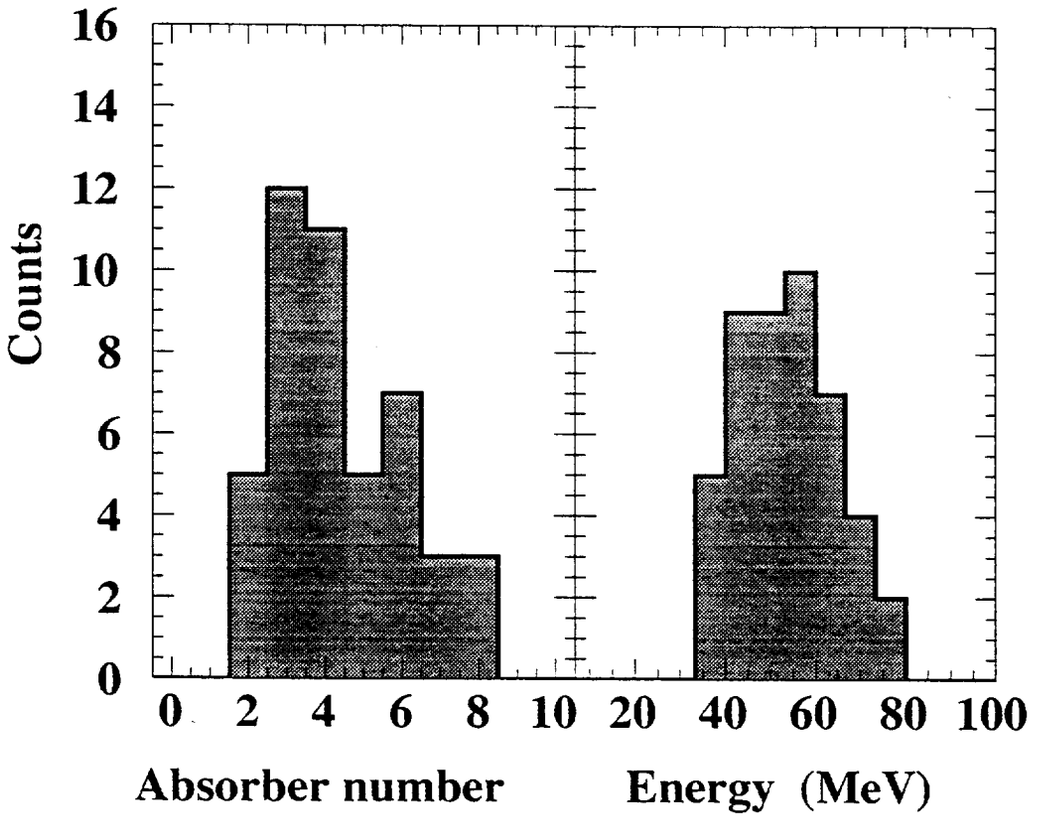
Counts
16
14
12
10
8
6
4
2
0
0 2 4 6 8 10 20 40 60 80 100
Absorber number
Energy (MeV)

Fig. 4

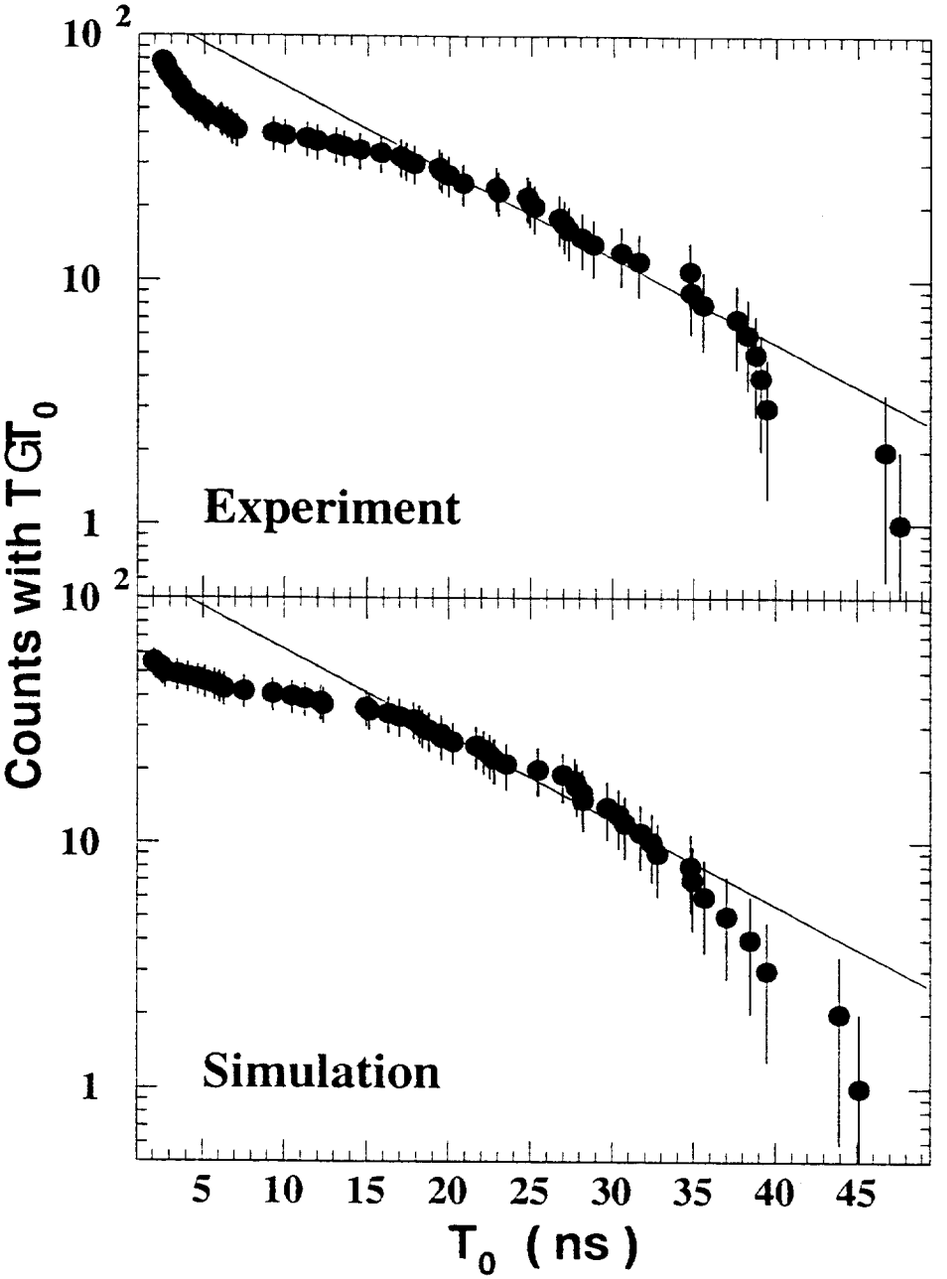
10 2
10
1
Experiment
10 2
10
1
Simulation
Counts with T>T0
5
10
15
20
25
30
35
40
45
T0 (ns)

Fig. 5

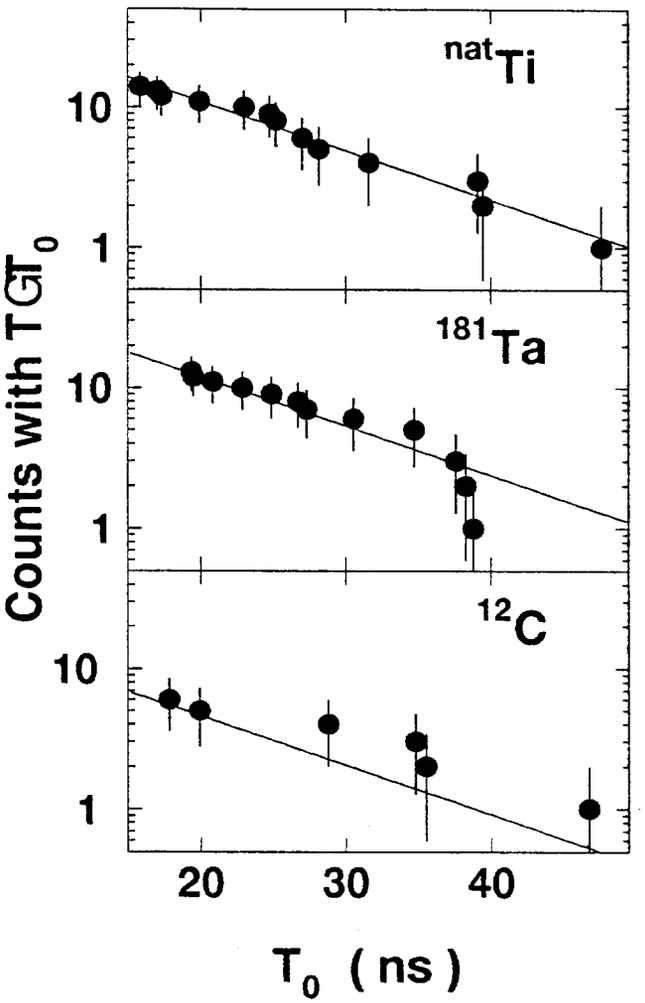

Fig. 6

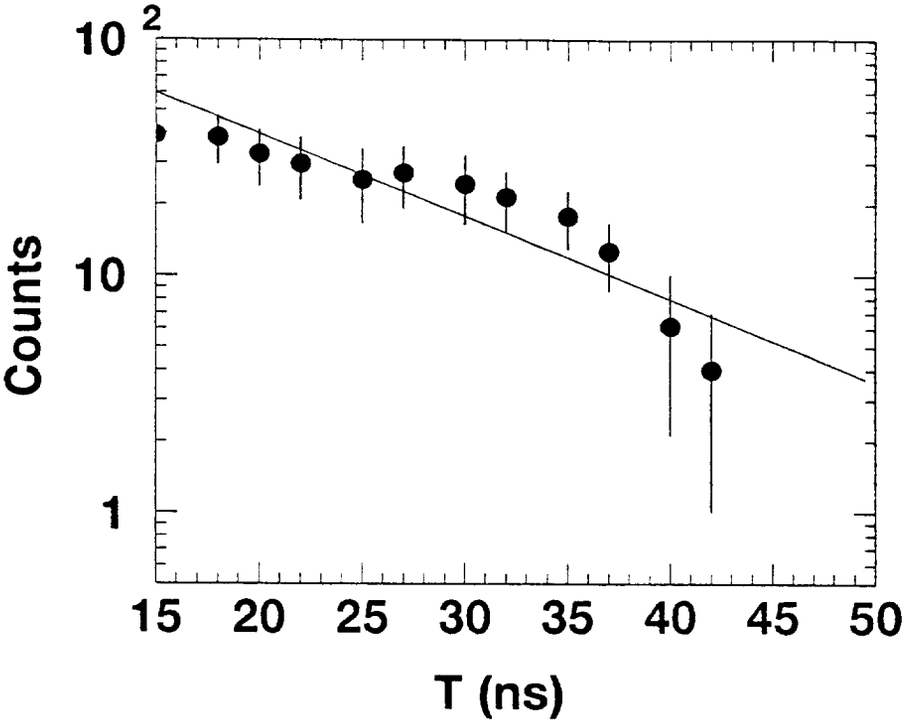

Fig. 7

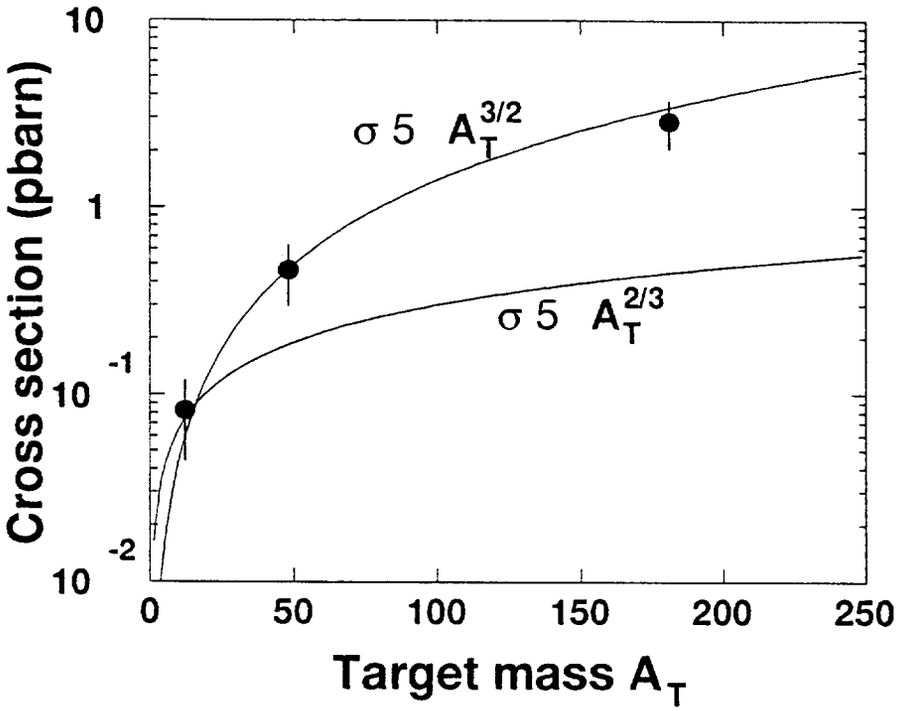
Cross section (pbarn)
10
1
-1
10
-2
10
σ 5 $A_T^{3/2}$
σ 5 $A_T^{2/3}$
0
50
100
150
200
250
Target mass A_T

Fig. 8

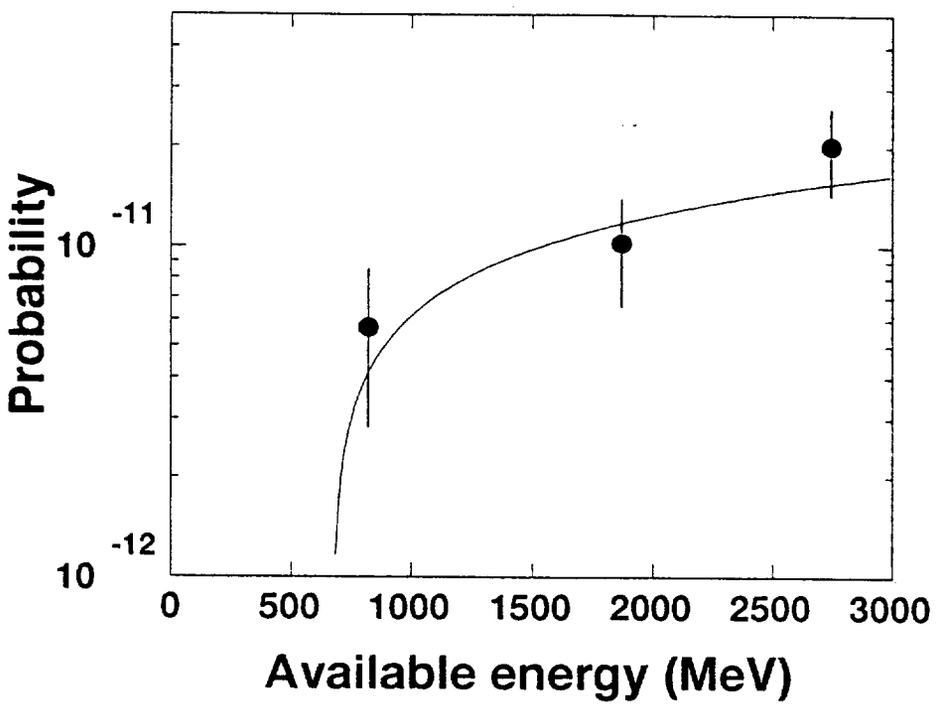
Probability
10 -11
10 -12
0
500
1000
1500
2000
2500
3000
Available energy (MeV)

Fig. 9

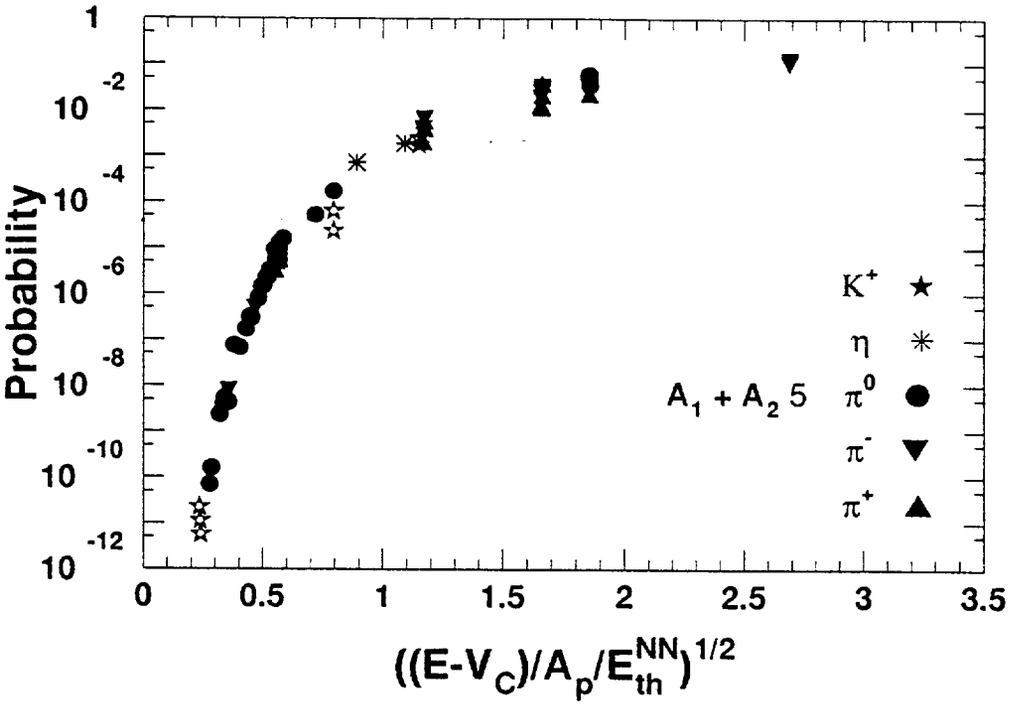
Probability
1
10^-2
10^-4
10^-6
10^-8
10^-10
10^-12
0
0.5
1
1.5
2
2.5
3
3.5
((E-V_C)/A_p/E_th^NN)^1/2
K+
η
A1 + A2 5
π0
π-
π+

Fig. 10

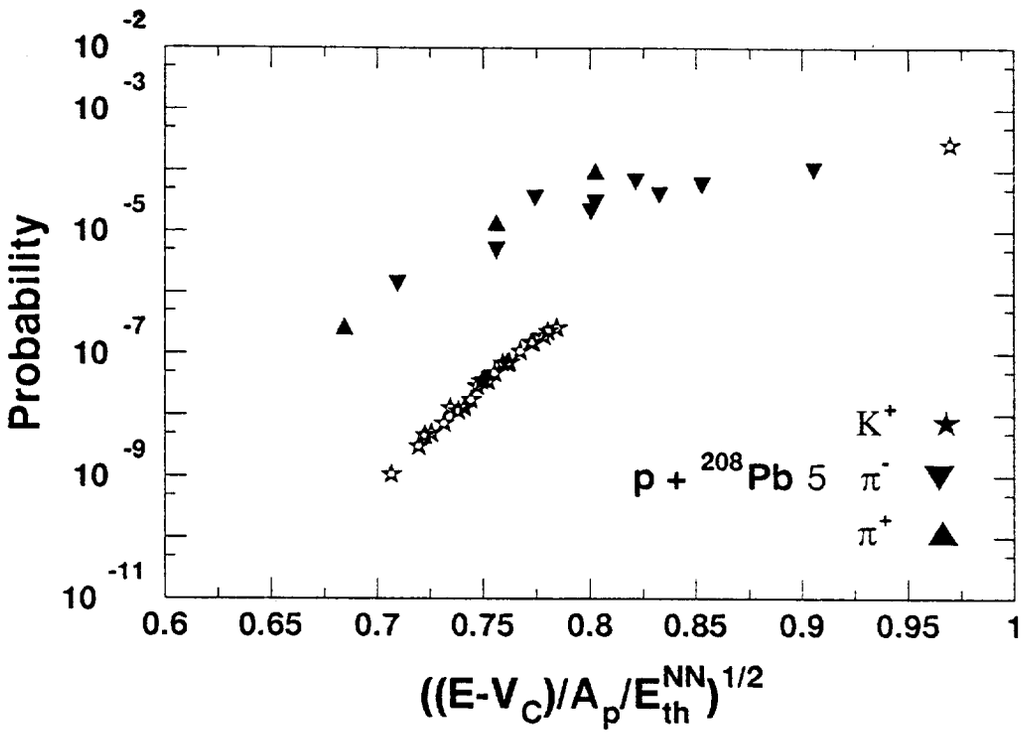
Probability
10^-2
10^-3
10^-5
10^-7
10^-9
10^-11
0.6
0.65
0.7
0.75
0.8
0.85
0.9
0.95
1
((E-V_C)/A_p/E_th^NN)^1/2
K+
p + 208Pb 5
π-
π+

Fig. 11

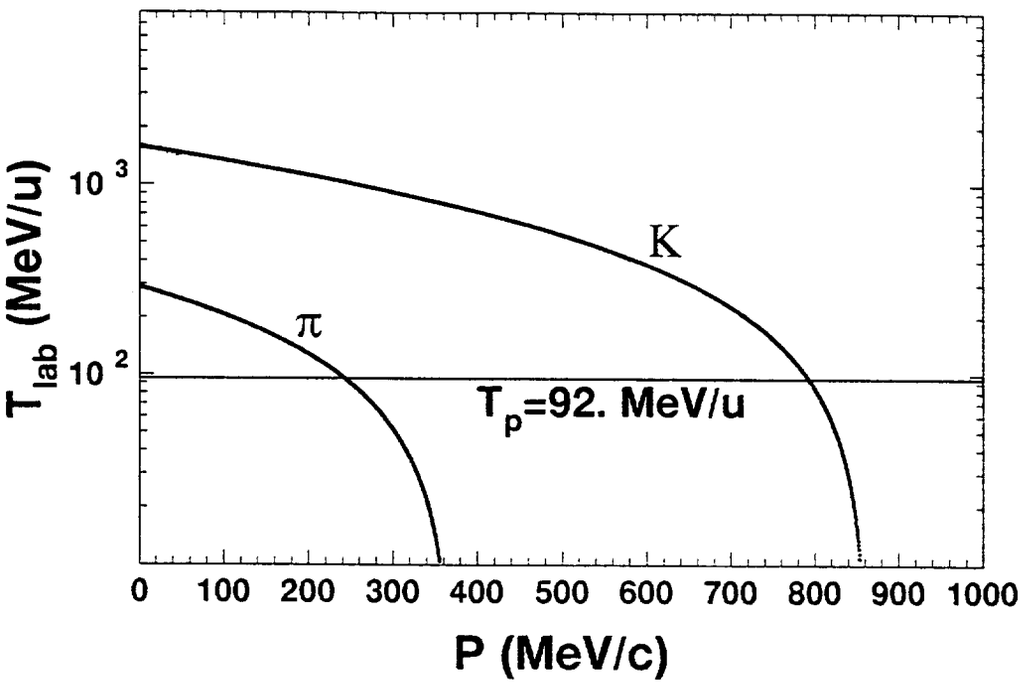
T_{lab} (MeV/u)
10^3
10^2
K
π
T_p=92. MeV/u
0
100
200
300
400
500
600
700
800
900
1000
P (MeV/c)

Fig. 12

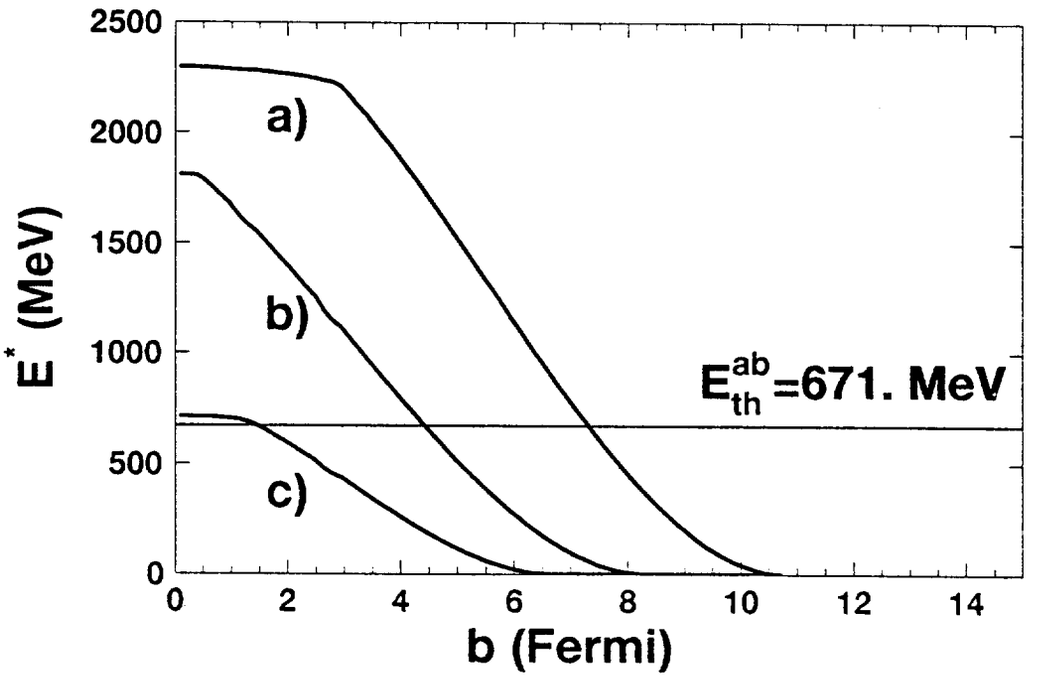
2500
2000
1500
1000
500
0
E* (MeV)
a)
b)
c)
E_{th}^{ab}=671. MeV
0
2
4
6
8
10
12
14
b (Fermi)

Fig. 13

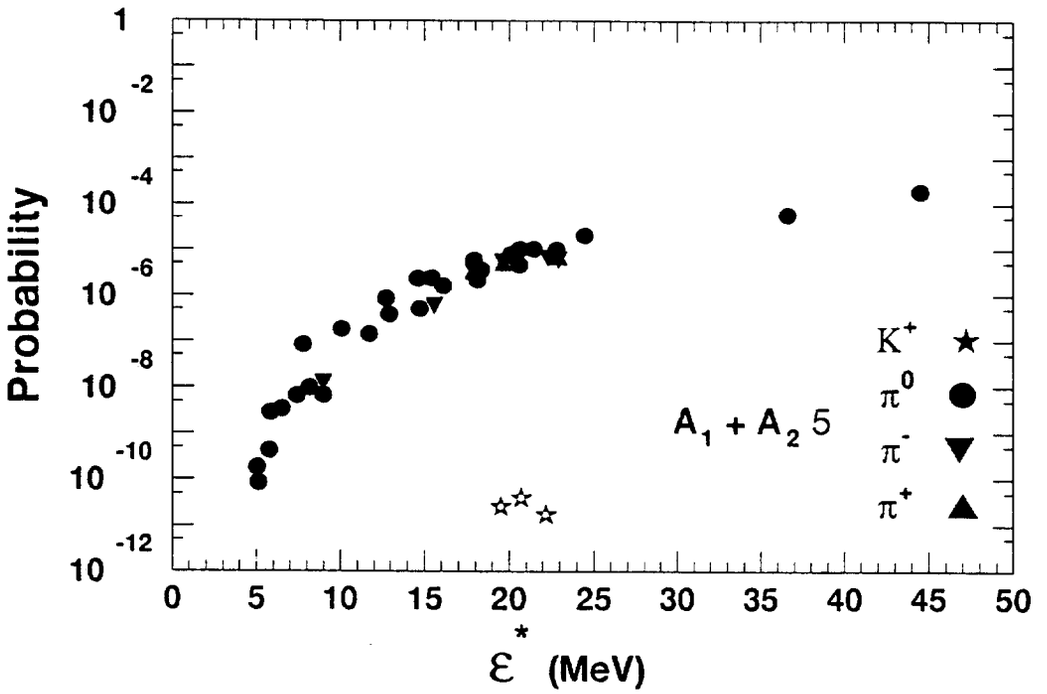
Probability
1
10 -2
10 -4
10 -6
10 -8
10 -10
10 -12
0 5 10 15 20 25 30 35 40 45 50
ε* (MeV)
A1 + A2 5
K+
π0
π-
π+

Fig. 14

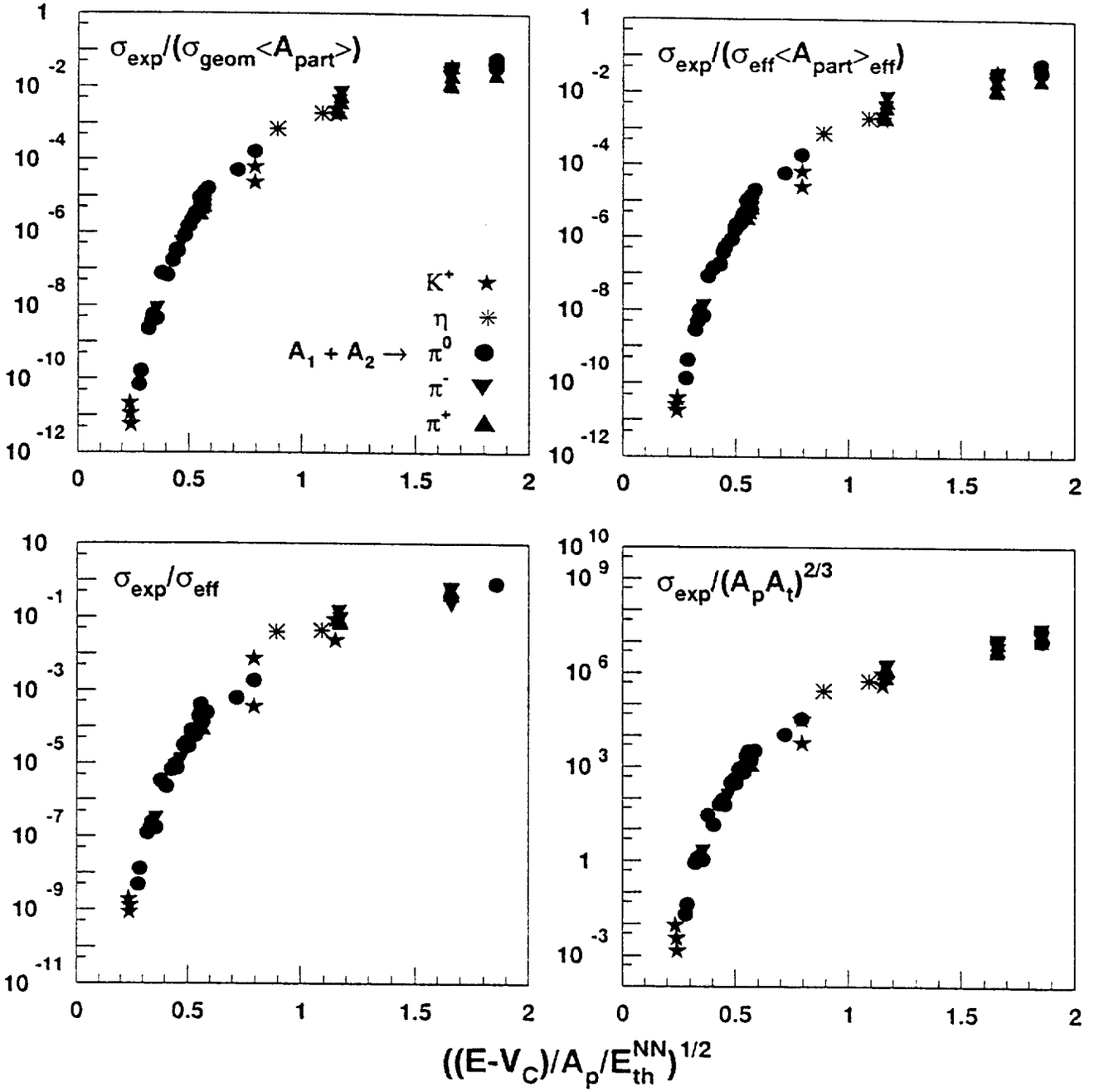
$\sigma_{exp}/(\sigma_{geom}<A_{part}>)$
$\sigma_{exp}/(\sigma_{eff}<A_{part}>_{eff})$
$\sigma_{exp}/\sigma_{eff}$
$\sigma_{exp}/(A_pA_t)^{2/3}$
$A_1 + A_2 \rightarrow$
K^+
η
π^0
π^-
π^+
$((E-V_C)/A_p/E_{th}^{NN})^{1/2}$

Fig. 15